Original article

Sanele Mngadi, Moganavelli Singh and Seipati Mokhosi*

PVA coating of ferrite nanoparticles triggers pH-responsive release of 5-fluorouracil in cancer cells

https://doi.org/10.1515/polyeng-2020-0271
Received October 6, 2020; accepted April 23, 2021;
published online June 7, 2021

Abstract: The use of magnetic nanoparticles (MNPs) has transformed both diagnostics and therapeutic approaches in cancer treatment. Along with developing novel anti-cancer drugs with high therapeutic potential, researchers are exploring innovative strategies for more targeted delivery in order to alleviate the associated potent side effects. In this study, we describe the synthesis of $Mg_{0.5}Co_{0.5}Fe_2O_4$ ferrite nanoparticles, their functionalisation with polyvinyl alcohol (PVA), and encapsulation of the anti-cancer drug 5-fluorouracil (5-FU). Functionalised nanoparticles viz. PVA-$Mg_{0.5}Co_{0.5}Fe_2O_4$ -5-FU displayed desirable physiochemical properties with regards to the spherical shape, hydrodynamic sizes of <120 nm and relative colloidal stability of up to <−33 mV. The drug encapsulating efficiency was found to be 68%. *In vitro* cytotoxicity profiles were determined using the MTT and SRB assays, with >65% cell death recorded in MCF-7 and HeLa cancer cell lines. Overall, the nanocomposites exhibited excellent physiochemical elements, high specificity towards cancerous cells and displayed pH-sensitive drug release in a simulated acidic tumour microenvironment. The encapsulation of 5-FU improved bioavailability of the drug in cancer cell lines for a prolonged duration, with the promise to enhance its therapeutic effect, biocompatibility and safety. These MNPs present as promising *in vitro* delivery systems that can be further developed for therapeutic applications.

Keywords: 5-fluorouracil; anti-cancer; cytotoxicity; magnetic nanoparticles; pH-responsive; PVA.

***Corresponding author: Seipati Mokhosi**, Discipline of Biochemistry, University of Kwazulu-Natal, Private Bag X54001, Durban, South Africa, E-mail: mokhosis@ukzn.ac.za
Sanele Mngadi and Moganavelli Singh, Discipline of Biochemistry, University of Kwazulu-Natal, Private Bag X54001, Durban, South Africa

1 Introduction

Magnetic nanoparticles (MNPs) are currently explored as competitive nanosystems of choice in the field of theranostics, with wide applications including bioseparation, magnetic resonance imaging, hyperthermia and drug delivery [1–4]. For effective delivery of therapeutics and drugs, important considerations are made of parameters *viz*. size, magnetism, biocompatibility and toxicity [3, 5]. Traditionally, iron oxide based magnetic NPs including magnetites (Fe_3O_4) and maghemites (γ-Fe_2O_3) have been duly opted because of their low toxicity profile [6, 7]. In recent years, ferrite NPs (MFe_2O_4) have presented as attractive NPs within the field of material synthesis and engineering with growing explorations in their biomedical applications. Cobalt ferrite ($CoFe_2O_4$) NPs are particularly interesting due to their unique physicochemical characteristics, tunable magnetic properties and ease of synthesis [8–10]. Doping these NPs with various other metal ions, such as magnesium, manganese and zinc into their lattices often gives rise to other new properties [9]. Use of bioactive compounds may confer favourable attributes such as improvement in biodegradability and lower cytotoxicities. Stability remains a significant challenge in biological environments including serum and physiological fluids as it impacts on cellular uptake and potential toxicity [11]. The nature of MNPs is such that the Van der Waals attractive forces between particles are often greater than the electrostatic repulsive forces which lead to aggregation [10, 11]. Further to this, the inherent often strong magnetic dipole–dipole interactions between the particles contribute to agglomeration [5, 11, 12]. Another critical disadvantage relates to non-specific destination of NPs which can lead to unwanted side effects [2, 13]. Incorporation of synthetic or natural polymers to the MNPs is often employed to address such challenges. Organic polymers such as polyethylene glycol (PEG) and polyvinyl alcohol (PVA) have been extensively reported to improve colloidal stability by introducing steric repulsion and limiting non-specific binding to cell receptors [11, 12]. The engineered

biocompatible polymer-coated MNPs facilitate adsorption or chemical linking of therapeutic agents to the particle surface for enhanced and targeted drug delivery at specific disease sites [14–16]. This is achieved as there is increased solubility of hydrophobic drugs, extension of the circulation of drugs in the blood and suppression of fast renal excretion [2, 13].

PVA is a very attractive hydrophilic synthetic polymer comprised of several reactive hydroxyl functional groups. It is extensively used in many industries, including the pharmaceutics and biomedicines [1] and confers important attributes such as biocompatibility [6, 17], biodegradability [18], low cytotoxicity [19], bactericidal effects [20] and adhesive properties [21]. 5-Fluorouracil (5-FU) is a hydrophilic, water soluble, antimetabolite drug that is used extensively in clinical chemotherapy for the treatment diverse cancers including breast, brain, liver, pancreatic and lung cancer [22, 23]. Free 5-FU presents heavy toxic side effects with minimal affinity to tumour cells and a short plasma half-life [24]. In order to reduce 5-FU associated side effects and improve its therapeutic index, incorporation of 5-FU into carriers has been accomplished thus selectively targeting cancer tissues for improved efficacy and safety [25].

In this study, we report on the synthesis, characterization and cytotoxicity studies of PVA coated MNPs *viz*. PVA-$Mg_{0.5}Co_{0.5}Fe_2O_4$. We have entrapped the anti-cancer drug 5-FU into PVA coating of MNPs and studied 5-FU loading and the drug release profile of MNPs, together with their possible *in vitro* specificity towards cancer cells.

2 Materials and methods

2.1 Materials

Cobalt chloride tetrahydrate ($CoCl_2{\cdot}4H_2O$, 98%), iron (III) chloride tetrahydrate ($FeCl_2{\cdot}4H_2O$, 98%), magnesium chloride hexahydrate ($Cl_2Mg{\cdot}6H_2O$, 99%), 5 M NaOH, $AgNO_3$, ethylene glycol ($(CH_2OH)_2$, 99%), polyvinyl alcohol (PVA), 5-fluorouracil (5-FU) and the dialysis tubing (MWCO 12,000 Da) were purchased from Sigma-Aldrich, St. Louis, MO, USA. 3-[(4,5-dimethylthiazol-2-yl)-2,5-diphenyl tetrazolium bromide] (MTT), sulforodhamine B (SRB Dye, $C_{27}H_{30}N_2O_7S_2$, Mw: 558.67 g mol^{-1}), phosphate-buffered saline tablets (PBS [140 mM NaCl, 10 mM phosphate buffer, 3 mM KCl]), acridine orange (AO) hemi (zinc chloride) salt [3,6-Bis(dimethylamino) acridine hydrochloride zinc chloride double salt] ($C_{17}H_{19}N_3$, Mw: 265.36, g mol^{-1}), ethidium bromide, glacial acetic acid and dimethyl sulfoxide (DMSO) were sourced from Merck (Darmstadt, Germany). Eagle's minimum essential medium (EMEM), L-glutamine (4.5 g L^{-1}), trypsin–versene and antibiotics (penicillin [10,000 U/mL], streptomycin [10,000 µg/mL] and amphotericin B [25 µg/mL]) were acquired from Lonza Bio-Whittaker (Walkersville, MD, USA). Fetal bovine serum (FBS) was used (Hyclone, UT, USA). Human embryonic kidney (HEK293) cells were sourced from the University of the Witwatersrand (Anti-viral Gene Therapy Unit, Johannesburg, South Africa. Human breast adenocarcinoma (MCF-7) and human cervical cancer (HeLa) cell lines were obtained from American Type Culture Collection (ATCC) (Manassas, VA, USA). All sterile tissue culture plasticware were obtained from Corning Inc. (New York, NY, USA). All biological assays were conducted under aseptic conditions in an airvolution class II biosafety laminar flow hood. Chemical reagents of analytical quality were used in this study without any further purification and ultrapure 18 MΩ Milli-Q water (pH 6.8) was used throughout.

2.2 MNP synthesis

$Mg_{0.5}Co_{0.5}Fe_2O_4$ NPs were synthesized using the glycol-thermal method, as previously reported [26]. Calculated stoichiometric measurements of 2.0818 g of $CoCl_2{\cdot}4H_2O$, 9.4854 g of $FeCl_2{\cdot}4H_2O$ and 1.0971 g of $Cl_2Mg{\cdot}6H_2O$ were weighed out and dissolved in 500 mL of deionized water. The homogenous solution was placed on a magnetic stirrer and the initial pH was recorded. The solution was stirred continuously for a duration of 30 min. Precipitation of the metal chlorides was carried out by the gradual addition of 5 M NaOH solution until a pH of 9 was reached. The precipitate was finally washed thoroughly to remove the unwanted chlorides. The wash steps were carried out using a Whatman (GF/F 110 mm) glass microfiber filter in a Buchner funnel. $AgNO_3$ was added to the washed solute to detect the presence of chlorides. A clear and non-cloudy solute indicated that all chlorides were removed. Thereafter, the washed precipitate was collected and submerged into 250 mL of ethylene glycol solution, and then placed in a PARR 4843 stirred pressure reactor and allowed to run for 6 h at a soak temperature of 200 °C with a stirring speed of 300 rpm and 80 psi pressure. The final product obtained was rinsed with 200 mL of ethanol over Whatman paper, and finally placed under a 200 W infrared light and allowed to dry overnight. The dried samples were then homogenized using an agate mortar and pestle.

2.3 Coating of MNPs

The synthesized $Mg_{0.5}Co_{0.5}Fe_2O_4$ MNPs were coated with PVA, with some modifications [27]. Briefly, 1 g of dry MNPs and 3 g of PVA were dissolved with vigorous stirring mechanically using an IKA RW 20 Digital Dual-Range Mixer System (Staufen, Germany) in deionized water at 80 °C, followed by a gradual decrease in temperature. The PVA-MNPs solution (MNPs: PVA = 1:3) were continuously stirred for 20 h at room temperature, then separated with a permanent magnet, washed 3 times with deionized water, and dried at room temperature. The PVA-coated MNPs (PVA-$Mg_{0.5}Co_{0.5}Fe_2O_4$) were then dispersed in a petri dish, left to dry at room temperature, and finally homogenized using an agate mortar and pestle.

2.4 Characterizations

Ultrastructural morphology was investigated via transmission electron microscopy (TEM) using a JEOL JEM-1010 TEM (Tokyo, Japan) operated at an accelerated voltage of 100 kV. The MegaView III Soft Imaging Systems (SIS) (JEOL JEM 1010, Tokyo, Japan) side-mounted 3-megapixel digital camera was used to document the micrographs. Images were captured using iTEM Soft Imaging Systems (SIS) megaview III fitted and

analyzed using analySIS LS Research v2.6 (Olympus Soft Imaging Solutions GmbH) to calculate the average nanoparticle diameter. The scanning electron microscopy (SEM) provided with details on the surface morphology of the nanoparticles. Samples were coated with gold using a Q150R Rotary-Pumped Sputter Coater (Leica Microsystems, Wetzlar, Germany). Viewing was done under a Zeiss Ultra Plus FE-SEM (ZEISS Field Emission Scanning Electron Microscope, Oberkochen, Germany) at a magnification of 3500×.

FTIR analysis via a Perkin Elmer Spectrum 100 FTIR (Fourier Transform Infrared) spectrometer (Waltham, MA, USA) was performed. A universal attenuated total reflectance (ATR) component was bound to it and MNPs were loaded onto the ATR crystal. This was followed by an exertion of pressure of 120 psi ensuring for maximum interaction between the nanoparticle samples and the crystal. Measurements were carried out at a range of 380–4000 cm^{-1} at a resolution of 4 cm^{-1} in room temperature at four scans per measurement. The data was generated using Spectrum® 10 Software. Zeta potential and hydrodynamic size distributions of the nanoparticles were measured using the nanoparticle tracking analysis (NTA) by the NanoSight NS500 (Malvern Instruments, Worcestershire, UK) at 25 °C. All samples were diluted 1:1000 in 18 Mohm water (pH 6.8) and the NTA software v3.0 (Malvern Instruments, Worcestershire, UK, 2014) was used to calculate the accurate hydrodynamic diameters using the Stokes–Einstein equation and the zeta potential using Smoluchowski approximation.

2.5 Drug encapsulation efficiency (EE)

The protocol for drug loading of the nanoparticles has previously been reported [28]. Briefly, the PVA coated $Mg_{0.5}Co_{0.5}Fe_2O_4$ was loaded with 5-FU, where 10 mg of nanoparticle powder was dissolved in 25 mL of a drug solution (0.2 mg/mL in PBS, pH 7.4). This was then placed on an orbital shaker at 200 rpm for 48 h at room temperature. In order to measure the drug EE, the drug-loaded nanocomposites PVA-$Mg_{0.5}Co_{0.5}Fe_2O_4$-5-FU were separated from the solution using an external magnetic field and oven-dried at 40 °C overnight. The concentration of 5-FU in the obtained supernatants was determined from a calibration curve by measuring the UV absorbance at 266 nm. The EE was estimated using the following equation:

$$\mathrm{EE}\,(\%) = 5\text{-}\mathrm{FU}_{\mathrm{total}} - 5\text{-}\mathrm{FU}_{\mathrm{supernantant}} / [5\text{-}\mathrm{FU}_{\mathrm{total}}] \times 100\%$$

2.6 Drug release studies

Briefly, 3 mg of the drug-loaded nanocomposites in 10 mL PBS were dispensed into dialysis tubings (12,000 MWCO) and suspended in separate beakers containing 20 mL of PBS (pH 4.5, 6.5 and 7.4, respectively). The solution was shaken continuously at 300 rpm at 37 °C. At specific time intervals, 2 mL of the dialysates were taken and the concentration of released drug was determined by measuring the UV–vis (ultraviolet visible) spectroscopy absorbance at 266 nm. Following each withdrawal, an equal volume of the dialysates was placed back into the aqueous medium to maintain the original PBS volume. The amount of drug released was plotted against time.

2.7 Cytotoxicity assays

The cytotoxicity of the nanocomposites was evaluated using the MTT and SRB assays in the normal HEK293 and cancerous MCF-7 and HeLa. Cells at a density of 2.0×10^4 per well were seeded in 96-well plates containing 100 µL growth medium (Eagles Minimum Essential Medium, EMEM) and incubated at 37 °C in a 5% CO_2 incubator for 24 h. Thereafter, the medium was replaced with a fresh medium, and cells were treated with varying concentrations of the nanoparticles and nanoconjugates for 48 h. An untreated positive cell control was included.

For the MTT assay, the spent medium was then removed, and fresh EMEM containing 10% MTT solution was added and cells incubated for 4 h at 37 °C, followed by removal of the medium/MTT solution and the addition of 100 µL DMSO. The absorbance at 540 nm was measured in a Mindray 96A microplate reader (Vacutec, Hamburg,Germany).

For the SRB assay, cells were fixed with 25 µL of cold 50% TCA (w/v), and then incubated for 1 h at 4 °C. Cells were then washed with distilled water, air dried, and stained with 50 µL SRB dye for 30 min at 37 °C. Stained cells were washed with 1% acetic acid, air dried, and the bound dye extracted with 100 µL of Tris buffer (10 mM, pH 10.5). Absorbance was read at 565 nm.

The percentage cell viability for both assays determined using the equation:

$$\%\ \text{Cell viability} = [\text{absorbance of treated cells} / \text{absorbance of untreated cells}] \times 100$$

2.8 Apoptosis assay

The acridine orange (AO)/ethidium bromide (EB) dual staining method [20] was used to investigate the effect of the pre-determined half maximal inhibitory concentrations (IC_{50}) of 5-FU encapsulated carriers on cell apoptosis. Briefly, cells (4.5×10^5 per well) were seeded in a 24-well plate and incubated for 24 h. Thereafter, the cells were exposed to the above samples for 24 h at 37 °C. Untreated cells were used as positive controls. Subsequently, cells were rinsed with cold PBS, and the dual stain (10 µL) (AO: 0.1 mg·ml^{-1}, EB: 0.1 mg·ml^{-1} in PBS) was added to the cells and allowed to stain for 5 min. Thereafter, the cells were briefly rinsed with cold PBS (200 µL) and viewed under an Olympus fluorescent microscope (200× magnification), and images were captured with a CC12 fluorescent camera (Olympus Co., Tokyo, Japan). The apoptotic index was estimated using the following equation:

$$\text{Apoptotic index} = \text{number of apoptotic cells} / \text{number of total cells counted}$$

2.9 Statistics

Statistical analysis of the data was carried out using two-way ANOVA and Tukey's multiple comparison test (GraphPad Instat 6) across all groups. Differences were considered statistically significant at $^{**}P < 0.01$ and $^{*}P < 0.05$.

3 Results and discussion

3.1 Physicochemical characterisations

The ultrastructural morphology, distribution and uniformity of all nanocomposites were examined using TEM. All the MNPs displayed a spherical morphology with

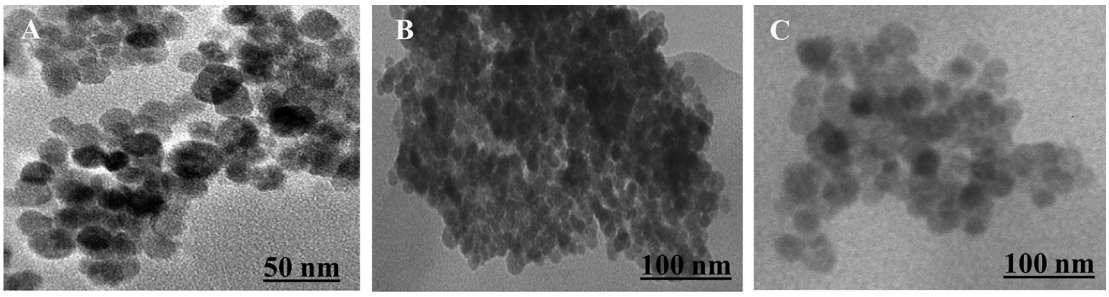

Figure 1: TEM images of (A) $Mg_{0.5}Co_{0.5}Fe_2O_4$, (B) PVA-$Mg_{0.5}Co_{0.5}Fe_2O_4$ and (C) PVA-$Mg_{0.5}Co_{0.5}Fe_2O_4$-5-FU NPs.

characteristic aggregation observed (Figure 1). The morphological features of the MNPs were similar to previously reported findings [27, 29, 30].

There was an evident increase in particle size from 11.55 to 18.9 nm upon functionalization with PVA and drug loading (Table 1). The NTA sizes obtained (Table 1) correlated with the trend observed for the TEM results but were notably higher as the particles are suspended in an aqueous medium. Swelling of the MNP's coating and aggregation in the aqueous media could have led to the larger sizes observed [11, 21]. Hydrodynamic sizes of <200 nm result in longer circulation times as the carrier can escape capture thus evading removal by macrophages in the biological system [31]. Coating with PVA increased the MNP average hydrodynamic size to 97.0 ± 5.4 nm, with a shift from a positive to a more negative ζ potential value (−33.6 ± 0.5 mV). The polydispersity index (PDI) measures NP heterogeneity, with values between 0.1 and 0.4 indicating moderately dispersed NPs. The uncoated NPs displayed a broad size distribution above 0.4. Coating with PVA resulted in improved size distribution of up to 0.24. With the value still below 0.3, these are deemed to be acceptable in drug delivery [32]. The observed highly negative ζ potential is probably due to the presence of negatively charged carboxylate ions on the surface of the MNPs. This finding was in keeping with similar results published on PVA-functionalised MNPs [33]. Further loading of 5-FU increased the size to 118.2 ± 14.3 nm with lowered but still negative ζ potential. At values higher than +30 mV or below −30 mV, this indicates a strong degree of electrostatic repulsion between adjacent similarly charged particles, leading to better colloidal dispersion [12]. Nanoparticles that are prone to agglomeration exhibit ζ potential less than 15 mV or above −15 mV [34]. With further optimisation, the drug-bearing nanostructures displayed the physiochemical properties adequate for use in delivery of therapeutics.

FTIR spectroscopy confirmed the chemical structure and functional groups present in $Mg_{0.5}Co_{0.5}Fe_2O_4$, PVA-$Mg_{0.5}Co_{0.5}Fe_2O_4$, 5-FU and PVA-$Mg_{0.5}Co_{0.5}Fe_2O_4$-5-FU (Figure 2). The spectra of the uncoated MNPs (Figure 2(A)) exhibited an absorption peak at ~3366 cm^{-1}, which corresponds to O–H stretching vibrations, while peak at ~1637 cm^{-1} belongs to H–O–H bending vibrations due to adsorbed water on the surface. The absorption band at ~533 cm^{-1} is attributed to the characteristic Fe-O bond of iron oxide NPs.

Coating with PVA as given in Figure 2(B), shows the absorption peaks at ~3233 cm^{-1} which are due to the stretching vibration of O–H band (alcoholic). The band at ~2939 cm^{-1} can be attributed to the CH_2 stretching vibration of the polymer linkage, and the additional peak at ~2339 cm^{-1} symmetric is sited for C–H stretching vibration with an additional peak observed at ~2339 cm^{-1} sited for C–H stretching vibration. The absorption peak at 1634 cm^{-1} revealed the H–O–H (δ) bending vibrations are a result of adsorbed water. Furthermore, the peaks at ~1428 and ~915 cm^{-1} are related to C–C stretching vibrations and CH_2 rocking, respectively. The peaks observed in the region of 1085–1150 cm^{-1} are typical of the C-O bending due to the

Table 1: TEM size, hydrodynamic size and zeta potential (ζ) of the synthesized MNPs.

	TEM size (nm)	Hydrodynamic size (nm)	PDI (SD/mean)^2	ζ (mV)
$Mg_{0.5}Co_{0.5}Fe_2O_4$	11.55	64.9 ± 49.9	0.42	1.3 ± 1.2
PVA-$Mg_{0.5}Co_{0.5}Fe_2O_4$	12.89	97.0 ± 5.4	0.17	−33.6 ± 0.5
PVA-$Mg_{0.5}Co_{0.5}Fe_2O_4$-5-FU	18.90	118.2 ± 14.3	0.24	−23.7 ± 0.1

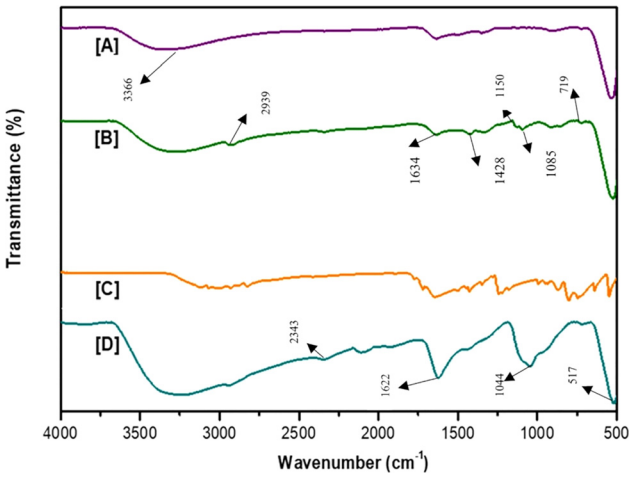

Figure 2: FTIR spectra of (A) $Mg_{0.5}Co_{0.5}Fe_2O_4$, (B) PVA-$Mg_{0.5}Co_{0.5}Fe_2O_4$, (C) 5-FU and (D) PVA-$Mg_{0.5}Co_{0.5}Fe_2O_4$-5-FU NPs.

alcohol moiety. The observed peaks corresponded to those reported in various literature and these vibrational bands confirmed the functionalization of the MNPs with PVA [27, 28, 35]. Pure 5-FU spectra (Figure 2(C)) showed N-H stretch at between 3222 and 2343 cm^{-1} and C=O stretch at ~1622 cm^{-1}. These same stretches were also seen in PVA-$Mg_{0.5}Co_{0.5}Fe_2O_4$-5-FU NPs therefore confirming an interaction of 5-FU and the PVA coated nanocarriers. The results of pure 5-FU in this study corresponds to the peaks of 5-FU observed in the literature [33, 34, 36, 37]. Interestingly, drug loaded nanocomposites (Figure 2(D)) displayed the signature stretching and deformation vibrations similar to PVA and 5-FU, suggesting successful loading of the drug. The drug carrier exhibited characteristic absorption peaks at ~3222 cm^{-1}, attributed to C-H stretching, and at ~ 1622 cm^{-1} ascribed to C=O amide band stretch vibrations. Further signals at ~ 1044 cm^{-1} due to C-O-C stretching and at ~ 719 cm^{-1} due to C-H plane vibrations. The contribution of metal is confirmed from the appearance of (M = Fe) band at 517 cm^{-1}. These results corroborated well with that of the TEM and NTA, confirming the successful loading and encapsulation of 5-FU within the PVA based nanocomposites.

3.2 Encapsulation efficiency (EE)

The efficacy of the drug delivery system to encapsulate 5-FU was determined through UV–vis spectroscopy, and the EE of 5-FU was found to be a satisfactory 68%. In a study using platinum–gold bimetallic nanoparticles, a 90.17% EE of 5-FU was attributed to the high ζ potential of the drug-complexed NP [34].

3.3 Release studies

The release of 5-FU NP from the drug loaded MNPs was investigated at pH 4.5, 6.5 and 7.4 as presented in Figure 3. At physiological pH 7.4, the results demonstrated a slow release of about 40% of 5-FU after 32 h rising to 51% after 48 h. At the slightest presence of acid (pH 6.5), the amounts released increased up to 65% after 48 h. A significantly higher release was however reported at the acidic pH 4.5, where 80% of 5-FU was released after 48 h. The trend observed showed investigated MNPs could be efficient in preventing undesired release of the drug in a physiological environment (pH 7.4), while achieving a rapid release in lower pH such as in cancer cells. This has been reported in earlier studies [38]. This would in turn, help to reduce the potent side effects of traditional chemotherapeutic drugs. The drug release in the acidic environment could be possibly due to the reduced electrostatic interactions between the drug molecules and the partly neutralized carboxylic groups on the surface of MNPs. This high drug released under acid pH was in correlation with previously reported studies [39, 40].

Potentially these nanocarriers not only minimize the adverse effects of the drug but also increase specific accumulation in the targeted tissue. This is advantageous for cancer therapy, because it specifically stimulates the release of 5-FU to the target site at low pH in tumours.

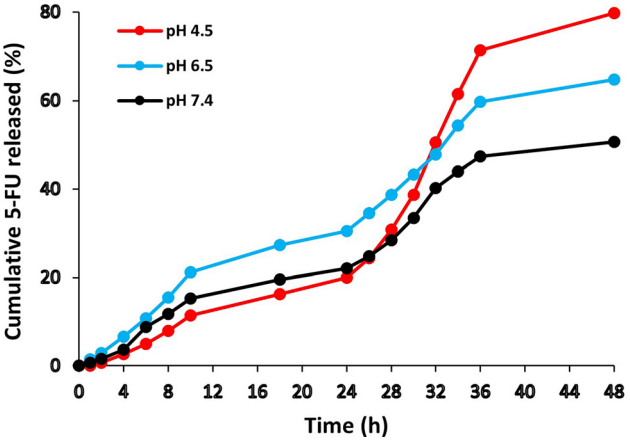

Figure 3: *In vitro* release profiles of 5-FU encapsulated PVA-$Mg_{0.5}Co_{0.5}Fe_2O_4$ nanocomposites at 37 °C.

3.4 Cytotoxic evaluation (MTT and SRB assays)

Preliminary toxicity screening *in vitro* is employed to investigate cell tolerability and toxicities to NP treatment. The level of toxicity exerted by MNPs *viz*. $Mg_{0.5}Co_{0.5}Fe_2O_4$, PVA-$Mg_{0.5}Co_{0.5}Fe_2O_4$ and PVA-$Mg_{0.5}Co_{0.5}Fe_2O_4$-5-FU was evaluated on selected human cell lines: Non-cancerous human embryonic kidney (HEK293), breast adenocarcinoma (MCF-7) and human cervical (HeLa) cell lines through the MTT and SRB assays (Figures 4 and 5). Principally, both assays were conducted to provide a reliable assessment of cytotoxicity, with each assay differing with regards to methodology, approach and sensitivity. The cytotoxicity profiles and IC_{50} values of PVA-$Mg_{0.5}Co_{0.5}Fe_2O_4$-5-FU and free drug (5-FU) are represented in Tables 2 and 3, respectively. Overall, similar trends in cytotoxicity in both assays were noted. Interestingly, non-drug bound MNPs exerted very low cytotoxicity even at the highest tested concentration (200 µg/ml) with >70% cell viability in all cells, thus suggesting good biocompatibility of these MNPs. Any cytotoxicity induced could have occurred through free radical-mediated DNA damage [34]. The non-drug bound MNPs produce cell viabilities similar to findings reported previously in literature [28, 38].

Exposure of cells to free 5-FU elicited a dose dependent decrease of cell survival, with non-cancer cells (HEK293) showing the lowest cell survival of ≤25% compared to the other two cancer cell lines (MCF-7 and HeLa) which displayed < 55% cell survival in both assays. Drug loaded nanocomposites exerted the most profound anti-proliferative effects in both cancer cells with up to 25% cell viability at the highest tested concentration in both assays correlating with report by Moustafa et al. [33]. The IC_{50} values of PVA-$Mg_{0.5}Co_{0.5}Fe_2O_4$-5-FU and 5-FU for the MCF-7 cells were approximately 126 µg/ml and 251 µg/mL in MTT assay, and 126 µg/mL and 501 µg/mL in the SRB assay, respectively with the nanocomposites displaying greater cytotoxicity than the free drug. Furthermore, the nanocomposites proved to be more effective in the HeLa cells, with lower IC_{50} values of approximately 100 µg/mL and 200 µg/mL (5-FU) in the MTT assay, and 126 µg/mL and 251 µg/mL in the SRB assay, respectively. The toxicity profiles obtained clearly supported enhanced cytotoxicity after 5-FU encapsulation. The nanocomposites executed the greatest anti-cancer activity in the HeLa cells than the MCF-7 cells, while demonstrating excellent tolerance in the non-cancer HEK293 cells. These results are in agreement with other studies of drug-loaded particles [33, 34, 41]. The results suggest that the loading of 5-FU to PVA-$Mg_{0.5}Co_{0.5}Fe_2O_4$ triggered a favourable synergistic effect that led to enhanced cytotoxicity.

Overall, drug loaded nanocomposites were well tolerated in the HEK293 cells with more than 65% cell viability, but instigated significantly greater damage in the cancer cells when compared to 5-FU at equivalent concentrations in both assays. These findings do correlate with the

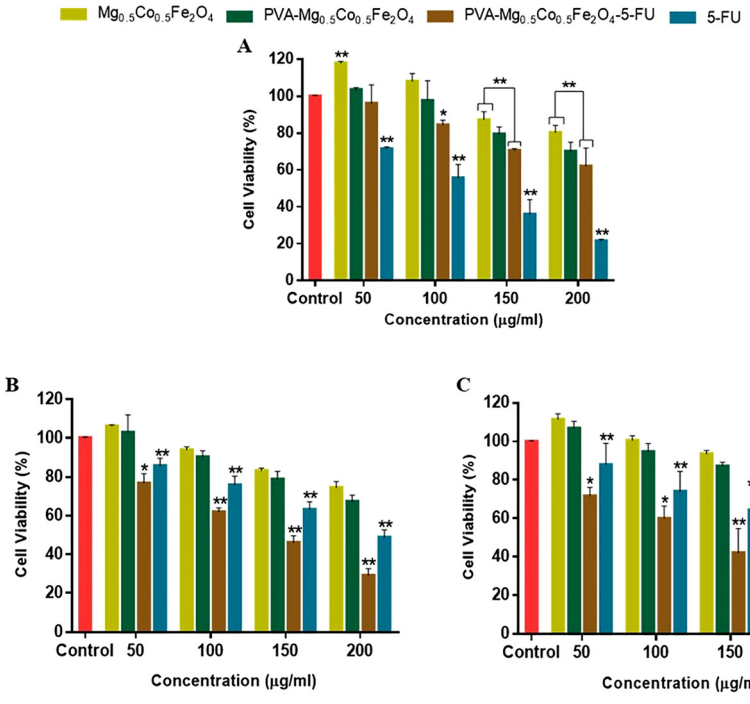

Figure 4: MTT cell viability assay *in vitro* in human cell lines. (A) HEK293, [B) MCF-7 and (C) HeLa.
$^{**}P < 0.01$, $^{*}P < 0.05$ was considered statistically significant. Data are represented as means ± SD ($n = 3$).

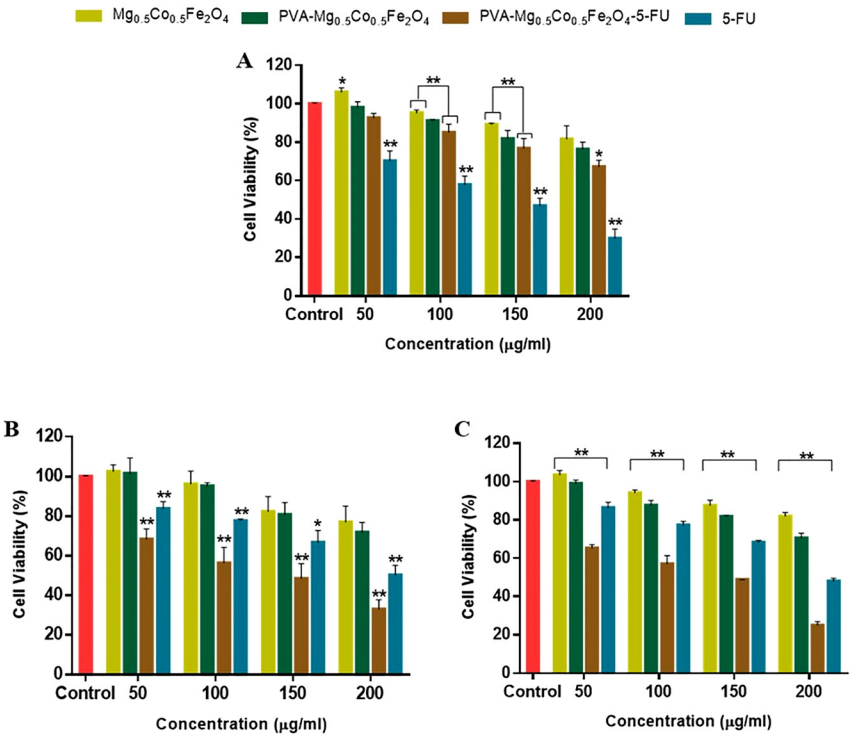

Figure 5: SRB cell viability assay *in vitro* in human cell lines (A) HEK293, (B) MCF-7 and (C) HeLa.
$^{**}P < 0.01$, $^{*}P < 0.05$ was considered statistically significant. Data are represented as means ± SD ($n = 3$).

Table 2: IC_{50} values of free 5-FU and 5-FU-loaded nanocomposites for HEK293, MCF-7 and HeLa cells.

Samples	IC_{50} calculation (μg/ml)		
	HEK293	MCF-7	HeLa
PVA-$Mg_{0.5}Co_{0.5}Fe_2O_4$-5FU	316	126	100
5-FU	100	251	200

Table 3: IC_{50} values of free 5-FU and 5-FU-loaded nanocomposites for HEK293, MCF-7 and HeLa cells.

Samples	IC_{50} calculation (μg/ml)		
	HEK293	MCF-7	HeLa
PVA-$Mg_{0.5}Co_{0.5}Fe_2O_4$-5-FU	251	126	126
5-FU	126	501	251

physiochemical characterisations and drug release profiles obtained. Basically, the combination of small size, high stability, improved tissue penetration, uptake via the cell membrane by endocytosis, and sustained 5-FU release within the tumour micro-environment, all contributed to the efficiency of the investigated anti-cancer nanoparticle formulation.

3.5 Apoptosis assay

The ability of the drug loaded nanocomposites to stimulate cancer cell death by apoptosis was investigated through the acridine orange/ethidium bromide (AO/EB) dual fluorescent staining method. Acridine orange permeates all cells resulting in the emittance of green fluorescence, whereas ethidium bromide is only taken up by non-viable cells that have lost their cytoplasmic membrane integrity causing the nucleus to fluoresce orange/red [42].

All control cells fluoresced green indicating healthy cells with an intact cell membrane (Figure 6(A), (D), and (G)). Conversely, all cells treated with 5-FU and 5-FU-MNP nanocomposites at their IC_{50} values, formed apoptotic bodies of varying degrees in all three cell lines (Table 3).

Noticeably, 5-FU induced high degrees of cell death in all cell lines through both apoptotic and necrotic pathways (Figure 6(C, (F), and (I)). The MNPs brought about regulated and cell specific cell death as nanocomposites displayed very low apoptotic indices in the HEK29)3 cells (0.12), with considerably higher indices in the two cancer cell lines (>0.45). The HeLa cells demonstrated a greater degree of sensitivity with higher apoptotic indices compared to the MCF-7 cells (Table 4). However, both cells exhibited characteristic apoptotic features. Overall, the apoptosis studies corroborated well with the MTT and SRB assays, as well as the drug release studies, and further

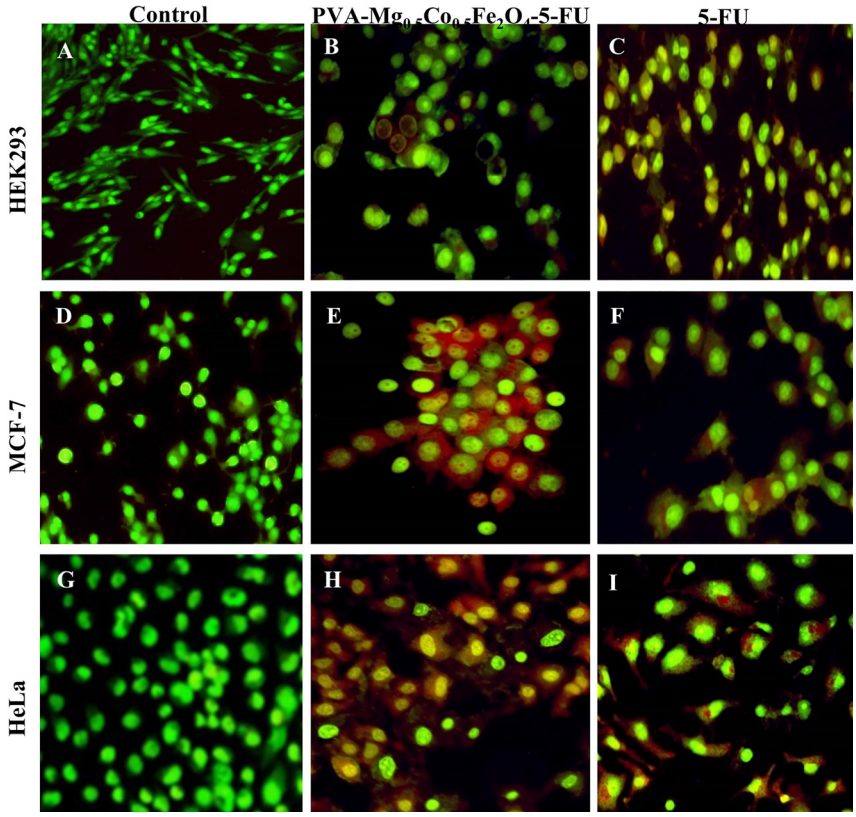

Figure 6: Fluorescent images of AO/EB stained cells.
(A) HEK293 control cells, (B) HEK293 cells treated with PVA-$Mg_{0.5}Co_{0.5}Fe_2O_4$-5FU NPs, (C) HEK293 cells treated with 5-FU (D) MCF-7 control cells, (E) MCF-7 cells treated with PVA-$Mg_{0.5}Co_{0.5}Fe_2O_4$-5FU NPs, (F) MCF-7 cells treated with 5-FU, (G) HeLa control cells, (H) HeLa cells treated with PVA-$Mg_{0.5}Co_{0.5}Fe_2O_4$-5-FU NPs and (I) HeLa cells treated with 5-FU. Images taken at 20× magnification.

Table 4: Apoptotic indices of free 5-FU and 5-FU-loaded nanocomposites.

Samples	Apoptotic indices		
	HEK293	MCF-7	HeLa
PVA-$Mg_{0.5}Co_{0.5}Fe_2O_4$-5FU	0.12	0.46	0.76
5-FU	0.42	0.23	0.37

confirmed the notion that pH-sensitive drug release brought about cell specific apoptosis induction, leading to favourable anti-cancer effects in the cancer cells investigated. 5-FU-MNPs not only reduced the toxic effects evident for the free 5-FU, but also enhanced the therapeutic efficacy towards cancer cells. These results further suggest the immense potential of these 5-FU-MNPs in cancer therapy.

4 Conclusion

We have successfully synthesized PVA functionalized MNPs encapsulated with the anti-cancer drug (5-FU) and investigated their pH-triggered drug release and anti-cancer activity for future application in cancer therapy. 5-FU-MNPs displayed good colloidal stability and small sizes (<200 nm) which is critical for drug delivery. 5-FU was quickly released in an acidic environment (pH 4.5–6.5), compared to a physiological environment (pH 7.4), suggesting cancer cell specificity and a pH-sensitive profile. Furthermore, this drug formulation enhanced drug accumulation at intercellular compartments of the cancer cells with low drug concentration in the normal cells. Moreover, the 5-FU-MNPs were less toxic to normal cells compared to free 5-FU, suggesting good biocompatibility of the MNPs with normal cells, which will prevent unwanted side effects during anti-cancer therapy. Thus, there is a therapeutic relevance attached to the use of PVA-MNPs with pH responsive behaviour and good biocompatibility, for 5-FU delivery in cancer therapy.

Author contributions: All the authors have accepted responsibility for the entire content of this submitted manuscript and approved submission.

Research funding: This work was supported by the National Research Foundation South Africa, 107407, 113850.

Conflict of interest statement: The authors declare no conflicts of interest regarding this article.

Compliance with ethical standards: No animals or human subjects were involved in this study.

References

1. Chomouka J., Drbohlavova J., Huska D., Adam V., Kizek R., Hubalek J. Magnetic nanoparticles and targeted drug delivering. *Pharmacol. Res.* 2010, *62*, 144–149.
2. Huang J., Li Y., Orza A., Lu Q., Guo P., Wang L., Yang L., Mao H. Magnetic nanoparticle facilitated drug delivery for cancer therapy with targeted and image-guided approaches. *Adv. Funct. Mater.* 2016, *26*, 3818–3836.
3. Kudr J., Haddad Y., Richtera L., Heger Z., Cernak M., Adam V., Zitka O. Magnetic nanoparticles: from design and synthesis to real world applications. *Nanomaterials* 2017, *7*, 243.
4. Sandler S. E., Fellows B., Mefford O. T. Best practices for characterization of magnetic nanoparticles for biomedical applications. *Anal. Chem.* 2019, *91*, 14159–14169.
5. Mahmoudi M., Sant S., Wang B., Laurent S., Sen T. Superparamagnetic iron oxide nanoparticles (SPIONs): development, surface modification and applications in chemotherapy. *Adv. Drug Deliv. Rev.* 2011, *63*, 24–46.
6. Umut E. Surface modification of nanoparticles used in biomedical applications in modern surface engineering treatments. In *Modern Surface Engineering Treatments*; Aliofkhazraei M., Ed. InTech: London, UK, 2013; pp. 185–208.
7. Galarreta I., Insausti M., de Muro I. G., de Larramendi I. R., Lezama L. Exploring reaction conditions to improve the magnetic response of cobalt-doped ferrite nanoparticles. *Nanomaterials* 2018, *8*, 63.
8. Momin N., Deshmukh A., Radha S. Synthesis and characterization of $CoFe_2O_4$ & $NiFe_2O_4$ magnetic nanoparticles for various biomedical applications: cell viability and cell death evaluations. *J. Nano Res.* 2015, *34*, 1–8.
9. Jauhar S., Kaur J., Goyal A., Singhal S. Tuning the properties of cobalt ferrite: a road towards diverse applications. *RSC Adv.* 2016, *6*, 97694.
10. Nasiri M., Hassanzadeh-Tabrizi S. A. Synthesis and characterization of folate-decorated cobalt ferrite nanoparticles coated with poly(ethylene glycol) for biomedical applications. *J. Chin. Chem. Soc.* 2018, *65*, 231–242.
11. Gutiérrez L., de la Cueva L., Moros M., Mazarío E., de Bernardo S., de la Fuente J. M., Morales M. P., Salas G. Aggregation effects on the magnetic properties of iron oxide colloids. *Nanotechnology* 2019, *30*, 1102001.
12. Socoliuc V., Peddis D., Petrenko V. I., Avdeev M. V., Susan-Resiga D., Szabó T., Turcu R., Tombácz E., Vékás L. Magnetic nanoparticle systems for nanomedicine -A materials science perspective. *Magnetochemistry* 2019, *6*, 2.
13. Arias L. S., Pessan J. P., Vieira A. P. M., de Lima T. M. T., Delbem A. C. B., Monteiro D. R. Iron oxide nanoparticles for biomedical applications: a perspective on synthesis, drugs, antimicrobial activity, and toxicity. *Antibiotics* 2018, *7*, 46.
14. Singh D., Mcmillan J. M., Kabanov A. V., Sokolsky-Papkov M., Gendelman H. E. Bench-to-bedside translation of magnetic nanoparticles. *Nanomedicine* 2014, *9*, 501–516.
15. Anselmo A. C., Mitragotri S. A review of clinical translation of inorganic nanoparticles. *AAPS J.* 2015, *17*, 1041–1054.
16. Ulbrich K., Hola K., Subr V., Bakandritsos A., Tucek J., Zboril R. Targeted drug delivery with polymers and magnetic nanoparticles: covalent and noncovalent approaches, release control, and clinical studies. *Chem. Rev.* 2016, *116*, 5338–5431.
17. Salunkhe A. B., Khot V. M., Thorat N. D., Phadatare M. R., Sathish C. I., Dhawale D. S., Pawar S. H. Polyvinyl alcohol functionalized cobalt ferrite nanoparticles for biomedical applications. *Appl. Surf. Sci.* 2013, *264*, 598–604.
18. Jonderian A., Maalouf R. Formulation and *in vitro* interaction of Rhodamine-B loaded PLGA nanoparticles with cardiac myocytes. *Front. Pharmacol.* 2016, *7*, 458.
19. Strehl C., Gaber T., Maurizi L., Hahne M., Rauch R., Hoff P., Häupl T., Hofmann-Amtenbrink M., Poole A. R., Hofmann H., Buttgereit F. Effects of PVA coated nanoparticles on human immune cells. *Int. J. Nanomed.* 2015, *10*, 3429–3445.
20. Tran N., Mir A., Mallik D., Sinha A., Nayar S., Webster T. J. Bactericidal effect of iron oxide nanoparticles on *Staphylococcus aureus*. *Int. J. Nanomed.* 2010, *5*, 277–283.
21. Couto D., Freitas M., Carvalho F., Fernandes E. Iron oxide nanoparticles: an insight into their biomedical applications. *Curr. Med. Chem.* 2015, *22*, 1808–1828.
22. Akinyelu J., Singh M. Folate-tagged chitosan-functionalized gold nanoparticles for enhanced delivery of 5-fluorouracil to cancer cells. *Appl. Nanosci.* 2019, *9*, 7–17.
23. Sun L., Chen Y., Zhou Y., Guo F., Zheng Y., Chen W. Preparation of 5-fluorouracil-loaded chitosan nanoparticles and study of the sustained release *in vitro* and *in viv*o. *Asian J. Pharm. Sci.* 2017, *12*, 418–423.
24. Tummala S., Satish Kumar M. N., Prakash A. Formulation and characterization of 5-Fluorouracil enteric coated nanoparticles for sustained and localized release in treating colorectal cancer. *Saudi Pharmaceut. J.* 2015, *23*, 308–314.
25. Fan Y. L., Fan B. Y., Li Q., Di H. X., Meng X. Y., Ling N. Preparation of 5-fluorouracil-loaded nanoparticles and study of interaction with gastric cancer cells. *Asian Pac. J. Cancer Prev. APJCP* 2014, *15*, 7611–7615.
26. Mngadi S. M., Mokhosi S. R., Singh M. Surface-coating of $Mg_{0.5}Co_{0.5}Fe_2O_4$ nanoferrites and their in vitro cytotoxicity. *Inorg. Chem. Commun.* 2019, *108*, 107525.
27. Nadeem M., Ahmad M., Akhtar M. S., Shaari A., Riaz S., Naseem S., Masood M., Saeed M. Magnetic properties of polyvinyl alcohol and doxorubicin loaded iron oxide nanoparticles for anticancer drug delivery applications. *J. PloS one* 2016, *11*, e0158084.
28. Mushtaq M. W., Kanwal F., Batool A., Jamil T., Zia-Ul-Haq M., Ijaz B., Huang Q., Ullah Z. Polymer-coated $CoFe_2O_4$ nanoassemblies as biocompatible magnetic nanocarriers for anticancer drug delivery. *J. Mater. Sci.* 2017, *52*, 9282–9293.
29. Geppert M., Hohnholt M., Gaetjen L., Grunwald I., Bäumer M., Dringen R. Accumulation of iron oxide nanoparticles by cultured brain astrocytes. *J. Biomed. Nanotechnol.* 2009, *5*, 285–293.
30. Bini R. A., Marques R. F. C., Santos F. J., Chaker J. A., Jafelicci (Jr). M. Synthesis and functionalization of magnetite nanoparticles with different amino-functional alkoxysilanes. *J. Magn. Magn Mater.* 2012, *324*, 534–539.
31. Suciu M., Ionescu C. N., Ciorita A., Tripon S. C., Nica D., Al-Salami H., Barbu-Tudoran L. Applications of superparamagnetic iron oxide nanoparticles in drug and therapeutic delivery, and biotechnological advancements. *Beilstein J. Nanotechnol.* 2020, *11*, 1092–1109.
32. Danaei M., Dehghankhold M., Ataei S., Davarani H. F., Javanmard R., Dokhani A., Khorasani S., Mozafari M. R. Impact of particle size and polydispersity index on the clinical applications of lipidic nanocarrier systems. *Pharmaceutic* 2018, *10*, 57.

33. Moustafa M. E., Amin A. S., Magdi Y. Cytotoxicity of 6-mercaptopurine via loading on PVA-coated magnetite nanoparticles delivery system: a new era of leukemia therapy. *J. Nanomed. Nanotechnol.* 2018, *9*, 521.
34. Maney V., Singh M. The synergism of platinum-gold bimetallic nanoconjugates enhances 5-Fluorouracil delivery *in vitro*. *Pharmaceutics* 2019, *11*, 439.
35. Guo Z., Zhang D., Wei S., Wang Z., Karki A. B., Li Y., Bernazzani P., Young D. P., Gomes J. A., Cocke D. L., Ho T. C. Interfacial layer and bulk nanocomposites thin film. *J. Nanoparticle Res.* 2010, *12*, 2415–2426.
36. Businova P., Chomoucka J., Prasek J., Hrdy R., Drbohlavova J., Sedlacek P., Hubalek J. Polymer coated iron oxide magnetic nanoparticles: preparation and characterization. In *Nanocon 2011*; Ostrava : Tanger, 2011: Brno, Czech Republic, 2011.
37. Udofot O., Affram K., Smith T., Tshabe B., Krishnan S., Sachdeva M., Agyare E. Pharmacokinetic, biodistribution and therapeutic efficacy of 5-fluorouracil-loaded pH-sensitive PEGylated liposomal nanoparticles in HCT-116 tumor bearing mouse. *J. Nat. Sci.* 2016, *2*, e171.
38. Mngadi S., Mokhosi S., Singh M., Mdlalose W. Chitosan-functionalized $Mg_{0.5}Co_{0.5}Fe_2O_4$ magnetic nanoparticles enhance delivery of 5-Fluorouracil *in vitro*. *Coatings* 2020, *10*, 446.
39. Prabha G., Raj V. Preparation and characterization of polymer nanocomposites coated magnetic nanoparticles for drug delivery applications. *J. Magn. Magn Mater.* 2016, *408*, 26–34.
40. Udofot O., Affram K., Israel B., Agyare E. Cytotoxicity of 5-fluorouracil-loaded pH-sensitive liposomal nanoparticles in colorectal cancer cell lines. *Integr. Cancer Sci. Ther.* 2015, *2*, 245.
41. Moodley T., Singh M. Polymeric mesoporous silica nanoparticles for enhanced delivery of 5-fluorouracil *in vitro*. *Pharmaceutics* 2019, *11*, 288.
42. Bezabeh T., Mowat M., Jarolim L., Greenberg A., Smith I. Detection of drug-induced apoptosis and necrosis in human cervical carcinoma cells using 1 H NMR spectroscopy. *Cell Death Differ.* 2001, *8*, 219.